Appendix A

Materials and Methods

All strains were constructed using standard *B. subtilis* protocols and molecular biology methods (Table A.1). The background of all strains used was *B. subtilis* PY79. For image segmentation, a constitutive promoter expressing fluorescent protein reporter RFP was chromosomally integrated into PY79 (LS1). Promoter fusions to fluorescent proteins were chromosomally integrated using *Bacillus* integration vectors pDL30, ECE174 (both from lab stocks), and pER82 (kindly provided by Jonathan Dworkin). We also used the antibiotic-switching plasmid ECE73 (*cmR*→*neoR*). The integration vector 174hs (from lab stock) containing the IPTG-inducible LacI system added to the ECE174 backbone was used to induce Spo0F to different levels. For copy number perturbation, the plasmid pHP13 (from lab stock) was used. Based on these, other plasmids for promoter fusions and for circuit perturbations were constructed with *Escherichia coli* DH5α or DH5αZ1 by using standard methods of PCR, restriction enzyme digests, and ligations (Table A.2, A.3),

i. The plasmid pSS938 was constructed by ligating the EcoRI-BamHI fusion PCR fragment P_{0A}-YFP and pDL30 cut with EcoRI-BamHI. The fusion PCR fragment P_{0A}-YFP was made by fusing P_{0A} (primers oss80967, oss80949 and template PY79) and YFP (primers oss80944, oss80147 from a template plasmid containing YFP from lab stock) using primers oss80967, oss80147.

ii. The plasmid pSS925 was constructed by ligating the BamHI-EcoRI fusion PCR fragment P_{0F}-CFP and ECE174 cut with EcoRI-BamHI. The fusion PCR fragment P_{0F}-CFP was made by fusing P_{0F} (primers oss80973, oss80972 and template PY79) and CFP (primers oss80975, oss80146 from a template plasmid containing CFP from lab stock) using primers oss100436, oss80146.

iii. The plasmid pSS711 was constructed by ligating the EcoRI-BamHI PCR fragment *spo0F* (primers oss80907, oss80181 and template PY79) and pHP13 cut with EcoRI-BamHI.

iv. The plasmid pSS1027 was constructed by ligating the EcoRI-BamHI fusion PCR fragment P_{hyp}-CFP and ECE174 cut with EcoRI-BamHI. The fusion PCR fragment P_{hyp}-CFP was made by fusing P_{hyp} (primers oss100801, oss100805 and template MF2158) and CFP (primers oss100804, oss100802 from a template plasmid containing CFP from lab stock) using primers oss100801, oss100802.

v. The plasmid pSS916 was constructed by ligating the EcoRI-BamHI fusion PCR fragment P_{0F}-YFP and pDL30 cut with EcoRI-BamHI. The fusion PCR fragment P_{0F}-YFP was made by fusing P_{0F} (primers oss80973, oss100437 and template PY79) and YFP (primers oss100438, oss80147 from a template plasmid containing YFP from lab stock) using primers oss100436, oss80147.

vi. The plasmid pSS1025 was constructed by ligating the EcoRI-BamHI fusion PCR fragment P_{0F}-YFP and pER82 cut with EcoRI-BamHI. The fusion PCR fragment P_{0F}-YFP was made as above.

vii. The plasmid pSS1031 was constructed by ligating the HindIII-NheI fusion PCR fragment Spo0F-CFP and 174hs cut with HindIII-NheI. The fusion PCR fragment Spo0F-CFP was amplified (primers oss100908, oss100905) from a vector already containing a Spo0F-CFP fragment, which was made by fusing the Spo0F gene (primers oss80900, oss80913 and template PY79) and CFP (primers oss80912, oss100802 from a template plasmid containing CFP from lab stock) using primers oss80900, oss100802.

viii. The *spo0F* deletion PCR was made by fusing the gene conferring *specR* with flanking regions bearing homology upstream and downstream of the Spo0F coding region. The primer pairs (oss80928, oss80924), (oss80922,oss80923) and (oss80925,oss80927) were used to PCR *specR* (pDL30 template), upstream homology region (PY79 template) and downstream homology region (PY79 template), respectively. These pieces were then fused using primers oss80922 and oss80927.

Number	Strain	Reference/Source/Construction
MF2158	PY79 *spo0A*::*specR*::*cmR* P_{lacI}-LacI P_{hyp}-$0A^{sad67}$	Lab stock
LS1	PY79 *ppsB*::*ermR* P_{trpE}-RFP	Lab stock
LS4	PY79	Lab stock
SS813	PY79 *ppsB*::*ermR* P_{trpE}-RFP *spo0A*::*specR*::*cmR* P_{lacI}-LacI P_{hyp}-$0A^{sad67}$	MF2158 → LS1
SS1039	PY79 *sacA*::*cmR* P_{hyp}-CFP	pSS1027 → LS4
SS1060	PY79 *sacA*::*cmR*::*neoR* P_{hyp}-CFP	ECE73 → SS1039
SS1075	PY79 *ppsB*::*ermR* P_{trpE}-RFP *spo0A*::*specR*::*cmR* P_{lacI}-LacI P_{hyp}-$0A^{sad67}$ *sacA*::*cmR*::*neoR* P_{hyp}-CFP	SS1060 → SS813
SS1125	PY79 *ppsB*::*ermR* P_{trpE}-RFP *spo0A*::*specR*::*cmR* P_{lacI}-LacI P_{hyp}-$0A^{sad67}$ *sacA*::*cmR*::*neoR* P_{hyp}-CFP *amyE*::*specR* P_{0A}-YFP	pSS916 → SS1075
SS1017	PY79 *ppsB*::*ermR* P_{trpE}-RFP *amyE*::*specR* P_{0F}-YFP	pSS938 → LS1
SS1019	PY79 *ppsB*::*ermR* P_{trpE}-RFP *amyE*::*specR* P_{0F}-YFP *spo0A*::*specR*::*cmR* P_{lacI}-LacI P_{hyp}-$0A^{sad67}$	MF2158 → SS1017
SS1106	PY79 *ppsB*::*ermR* P_{trpE}-RFP *amyE*::*specR* P_{0F}-YFP *spo0A*::*specR*::*cmR* P_{lacI}-LacI P_{hyp}-$0A^{sad67}$ *sacA*::*cmR*::*neoR* P_{hyp}-CFP	SS1060 → SS1019
SS946	PY79 *ppsB*::*ermR* P_{trpE}-RFP *sacA*::*cmR* P_{0F}-CFP	pSS925 → LS1
SS1007	PY79 *ppsB*::*ermR* P_{trpE}-RFP *sacA*::*cmR* P_{0F}-CFP *amyE*::*specR* P_{0A}-YFP	pSS916 → SS946
SS1021	PY79 *ppsB*::*ermR* P_{trpE}-RFP *sacA*::*cmR*::*neoR* P_{0F}-CFP *amyE*::*specR* P_{0A}-YFP	ECE73 → SS1007
SS1023	PY79 *ppsB*::*ermR* P_{trpE}-RFP *sacA*::*cmR*::*neoR* P_{0F}-CFP *amyE*::*specR* P_{0A}-YFP pHP13-*spo0F*	pSS711 → SS1021
SS745	PY79 *spo0F*::*specR*	*spo0F* deletion PCR → LS4
SS843	PY79 *ppsB*::*ermR* P_{trpE}-RFP *spo0F*::*specR*	SS745 → LS1
SS1037	PY79 *ppsB*::*ermR* P_{trpE}-RFP *spo0F*::*specR* *amyE*::*neoR* P_{0F}-YFP	pSS1025 → SS843
SS1064	PY79 *ppsB*::*ermR* P_{trpE}-RFP *spo0F*::*specR* *amyE*::*neoR* P_{0F}-YFP *sacA*::*cmR* P_{lacI}-LacI P_{hyp}-Spo0F-CFP	pSS1031 → SS1037

Table A.1: List of strains.

Number	Plasmid
pSS916	pDL30 P_{0A}-YFP
pSS925	ECE174 P_{0F}-CFP
pSS711	pHP13-*spo0F*
pSS1027	ECE174 P_{hyp}-CFP
pSS938	pDL30 P_{0F}-YFP
pSS1031	174hs Spo0F-CFP
pSS1025	pER82 P_{0F}-YFP

Table A.2: List of plasmids.

Number	Primer Sequence (5'-3')
oss80146	ATA GAATTC AAAAGGCTGAACCCTAAGGT
oss80147	GAT GGATCC GCAATGATGAACCAGTAAGAGTAGC
oss80967	ACT GAATTC CAGAAGCAGGAATCGATATTTATGG
oss80949	CAACGCCGGTGAACAGTTCTTCACCTTTGCTCAT GTTTCTTCCTCCCCAAATGTAGTTAA
oss80944	GTGAATCCTGTTAACTACATTTGGGGAGGAAGAAAC ATGAGCAAAGGTGAAGAACTGTTC
oss80973	GGCCTGCTGGTAATCGCAGGCCTTTTTTATT AATCCTCCTTTATAACGTACAATATCAGTA
oss100436	CAC GGATCC GGCCTGCTGGTAATCGCAGGCCTTTTTTATTAATCCTCCTTTATAACGTACA
oss80972	AACTCCAGTGAAAAGTTCTTCTCCTTTACGCAT ATTCATCATTTTACACCCCAATATTAT
oss80975	CGAAAATCATAATATTGGGGTGTAAAATGATGAAT ATGCGTAAAGGAGAAGAACTTTTCA
oss80907	AGC GGATCC AAGTGAATCCTCCTTTATAACGTACAATA
oss80181	ATA GAATTC GTCAGTTAGACTTCAGGGGCAGAT
oss100801	TAT GAATTC GACTCTCTAGCTTGAGGCATCAAATAA
oss100805	AACTCCAGTGAAAAGTTCTTCTCCTTTACGCAT AGTAGTTCCTCCTTATGTGTCGACTAA
oss100804	AATTAAGCTTAGTCGACACATAAGGAGGAACTACT ATGCGTAAAGGAGAAGAACTTTTCA
oss100802	ATA GGATCC AAAAGGCTGAACCCTAAGGT
oss100436	CAC GAATTC GGCCTGCTGGTAATCGCAGGCCTTTTTTATT AATCCTCCTTTATAACGTACA
oss100437	AACGCCGGTGAACAGTTCTTCACCTTTGCTCAT ATTCATCATTTTACACCCCAATATTAT
oss100438	ACGAAAATCATAATATTGGGGTGTAAAATGATGAAT ATGAGCAAAGGTGAAGAACTGTTC
oss100908	ATA AAGCTT ACATAAGGAGGAACTACT ATGATGAATGAAAAAATTTTAATCGTTG
oss100905	ATA GCTAGC AAAAGGCTGAACCCTAAGGT
oss80900	ATA GAATTC AGTGAATCCTCCTTTATAACGTACAATAT
oss80913	TGAAAAGTTCTTCTCCTTTACGCATGTTAGACTTCAGGGGCAGATATTTT
oss80912	AAAATATCTGCCCCTGAAGTCTAAC ATGCGTAAAGGAGAAGAACTTTTCA
oss80922	TATCAGGATGAAGTGGTGTACGAGC
oss80927	TAACTGTTTCTTTGATCGCTTCACG
oss80924	CGAAAATCATAATATTGGGGTGTAAACATATGCAAGGGTTTATTGTTTTCTAA
oss80923	TTAGAAAACAATAAACCCTTGCATATGTTTACACCCCAATATTATGATTTTCG
oss80925	ATGTATTCACGAACGAAAATCGATCAAAAAGAAGAAACAAATGAATCATG
oss80928	CATGATTCATTTGTTTCTTCTTTTTGATCGATTTTCGTTCGTGAATACAT

Table A.3: List of primers.

Appendix B

Movie Protocols

Time-lapse microcopy. Cells to be imaged were inoculated in CH media and grown overnight in a 30°C shaking water incubator. They were then diluted 1:40 into fresh CH media and grown for 2–3 hours so that the OD600 was in the range 0.5–0.7. Following this, they were resuspended 1:1 in Sterlini-Mandelstam (SM) media after two washes in SM. 0.5ul of this was spotted on an appropriate pad (0.5mm x 0.5mm), allowed to dry, and flipped onto a glass-bottom dish (Wilco). The dish was sealed with parafilm to reduce pad evaporation during imaging. The pads were made from SM media mixed with 1.5% Low Melting Point Agarose (Omni). Required amount of inducer IPTG was added to the pads.

Progression to sporulation was imaged at 37°C using a microscope automated for time-lapse fluorescence data acquisition. Images were acquired every 10 minutes on a Nikon Eclipse-Ti inverted microscope fitted with a perfect focus system, ASI motorized stage, Photometrix Coolsnap HQ2 camera, Sutter Lambda LS Xenon Arc lamp, and controlled from a computer using MetaMorph.

Data analysis. The fluorescence values and lengths in single cells were extracted with customized segmentation and tracking algorithms coded in MATLAB and C. Promoter activity per unit length (P) was calculated from the measured mean fluorescence value (M) and cell lengths (L) using the formula

$$P(t) = \frac{dM}{dt} + \frac{1}{L}\frac{dL}{dt}M(t).$$

The derivative was computed from a smoothened version of the mean fluorescence and cell length. For this, mean fluorescence was smoothened with a moving average filter and length

was fitted to a second-order polynomial. To plot the transcriptional bandpass characteristics, time traces up to the initiation of sporulation, as seen from the appearance of a fluorescent dark spot at the tip of the cell, were used. For the post-translational bandpass, the peak P_{0F} pulse amplitude was measured from $T = 0$ minutes to $T = 600$ minutes, and the steady state Spo0F-CFP level was measured at $T = 500$ minutes. For measurements of phase shift between P_{0A} and P_{0F}, promoter activity pulses with peak amplitude greater than a threshold ($0.1 a.u.$) were used.

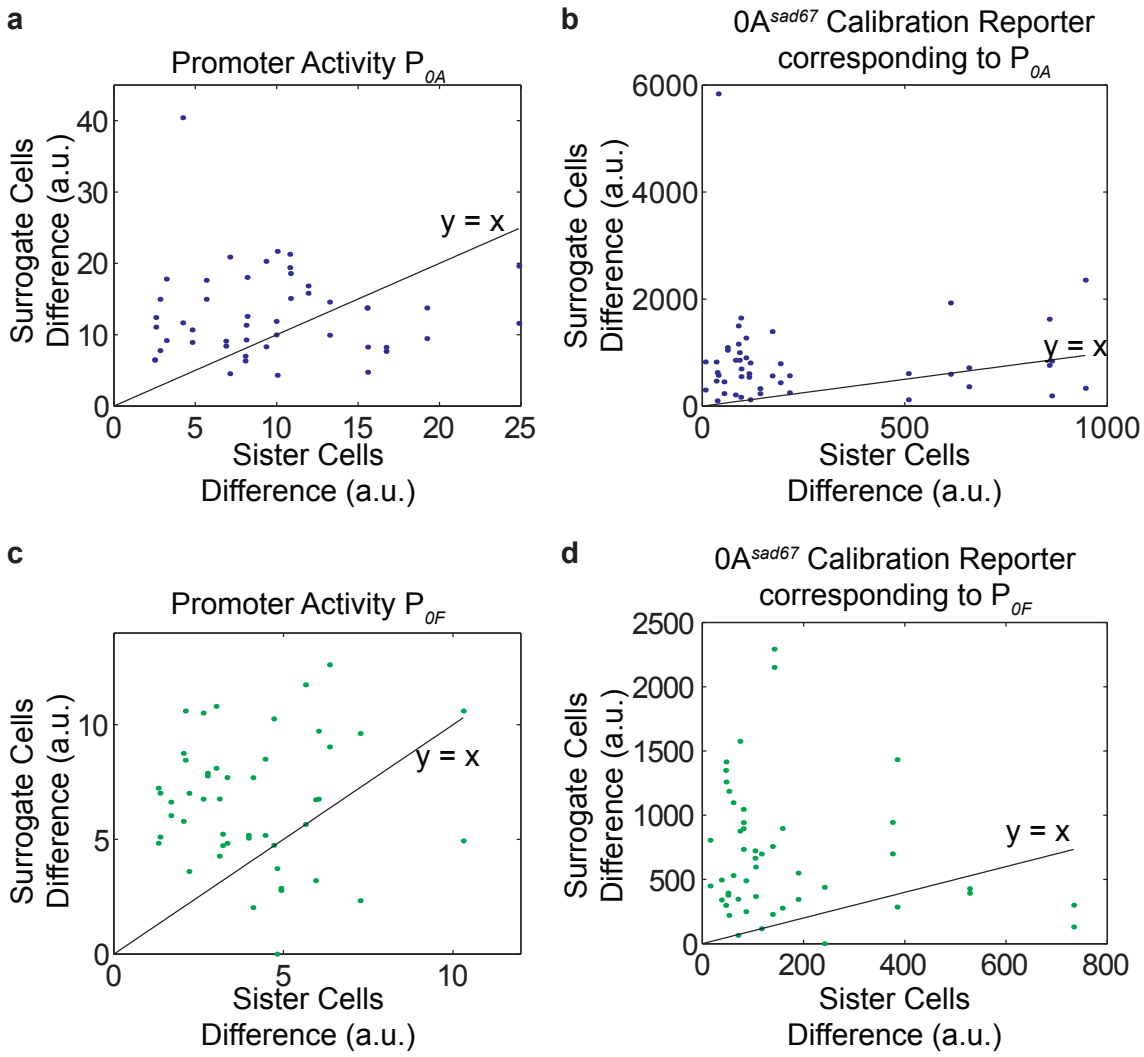

Figure B.1: Variability between sister cells is typically smaller than between randomly chosen sister cell pairs. Difference between a cell and its sister and between the same cell and a randomly chosen surrogate sister cell is calculated for traces of (a) P_{0A}, (b) Spo0A^{sad67} calibration reporter corresponding to the P_{0A} bandpass measurement, (c) P_{0F}, and (d) Spo0A^{sad67} calibration reporter corresponding to the P_{0F} bandpass measurement. Each dot represents one cell, and has co-ordinates (x, y), where x is the difference between sister cells and y is the difference between surrogate cells. Difference metric for two given traces $u(t)$ and $v(t)$ is, $d(u, v) = \sum_{t=0}^{T} |u(t) - v(t)|$, where T is the minimum of the durations of the two traces. In each case, most points lie above the straight line $y = x$, indicating that the difference between sister cells is smaller than between surrogate sister cells.

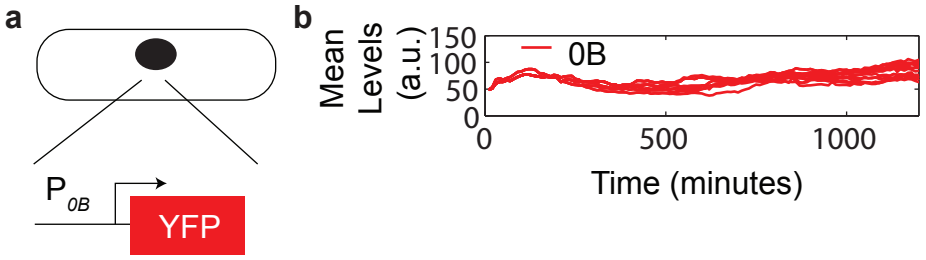

Figure B.2: Mean fluorescence of a P_{0B} reporter changes less than twofold during sporulation initiation. (a) Schematic of the strain with a YFP fluorescent reporter fused to P_{0B}. The strain uses the plasmid ECE174 P_{0B}-YFP (from lab stocks) integrated into an LS1 background. Imaging was done as described in the methods section, but on an Olympus IX-81 inverted microscope fitted with an ASI motorized stage, Hamamatsu Orca-ER camera, Sutter Lambda LS Xenon Arc lamp, and controlled using a combined Visual Basic - ImagePro software. (b) Mean fluorescence levels are non-zero at the start and change less than twofold during sporulation initiation.

Appendix C

Analysis of Models

Mathematical modeling was done in MATLAB. Nullclines in the two-dimensional model were computed from the zero contour of the surface functions $P_{0A}(A_T, F_T) - \gamma A_T$ and $P_{0F}(A_T, F_T) - \gamma F_T$. Ordinary differential equations were solved in MATLAB using integrator ode23s. The dependence of Spo0A∼P on Spo0F levels in the model without feedback and pulsing was computed by simulating the equations for a time longer than the timescale of the system. In the simulation of the two-dimensional model, A_p was computed at each timestep by simulating the equation of the phosphorylated proteins using the current values of A_T, B_T, F_T, K_T, and $k_s(ON/OFF)$.

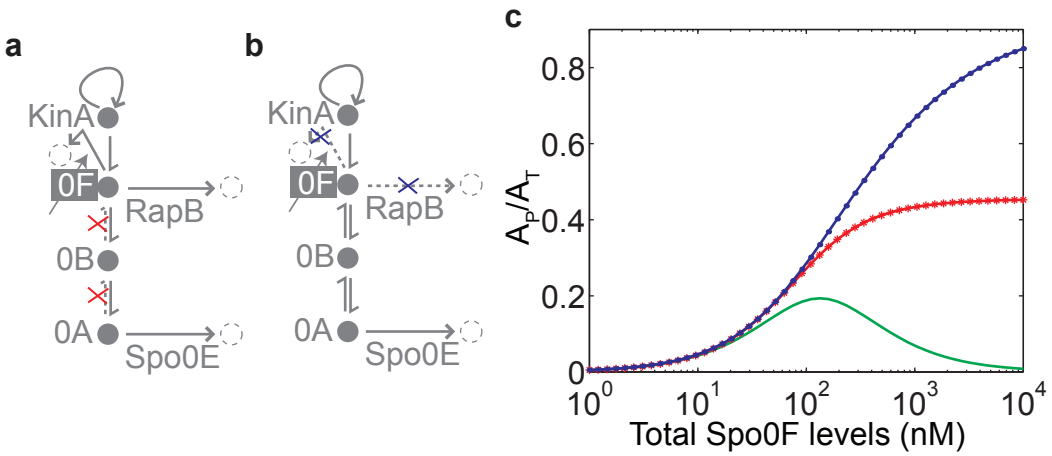

Figure C.1: Post-translational bandpass in the model is due to drain of Spo0A phosphates via reverse phosphotransfer and Spo0F phosphatases. Diagrams of the core phosphorelay with no reverse phosphotransfer (a, red) and no Spo0F phosphatase (b, blue), for which the post-translational Spo0F bandpass computation is performed from the simple phosphorelay model (no pulsing or transcriptional feedbacks). Both curves are plotted in (c), along with the curve from Fig. 2.4 (green).

Post-translational Spo0F bandpass in a more complex model of the core phosphorelay. This supplementary information describes a model of core phosphorelay with a more complicated reaction scheme that that described in the main text. The post-translational Spo0F bandpass discussed in the main text is based on a simple model of the core phosphorelay. In principle, a more complicated reaction scheme involving reaction intermediates is also possible. Here, we verify the post-translational Spo0F bandpass results in a model of the core phosphorelay that contains these reaction intermediates. Such reaction schemes have been previously used for phosphorelay-like signaling systems [54]. This model consists of 17 variables, of which eight correspond to the phosphoforms of the four phosphorelay proteins — K, K_p, F, F_p, B, B_p, A, A_p. In addition there are two additional variables corresponding to the free levels of the phosphatases of Spo0A and Spo0F, denoted E and R, respectively. Finally, there are seven additional variables corresponding to the reaction intermediates involved in the phosphorylation, phosphotransfer, and dephosphorylation reactions — $[K_pF]$, $[F_pB]$, $[B_pA]$, $[KT]$, $[KTF_p]$, $[F_pR]$, $[A_pE]$. Here, the variable T denotes ATP, which is assumed to be maintained at a constant value by the cell. Consequently, $[KT]$ is the KinA-ATP intermediate that mediates autophosphorylation and $[KTF_p]$ is the $[KT]$-Spo0F intermediate that mediates the dephosphorylation of Spo0F. These variables are not independent as they are constrained by the total concentrations of these proteins. There are six such constraints,

$$\begin{aligned}
A_T &= A + A_p + [B_pA] + [A_pE], \\
B_T &= B + B_p + [B_pA] + [F_pB], \\
F_T &= F + F_p + [F_pB] + [K_pF] + [KTF_p] + [F_pR], \\
K_T &= K + K_p + [KTF_p] + [K_pF] + [KT], \\
R_T &= [F_pR] + R, \\
E_T &= [A_pE] + E.
\end{aligned}$$

Here, A_T, B_T, F_T, K_T, R_T, and E_T denote the total concentrations of Spo0A, Spo0B, Spo0F, KinA, RapB, and Spo0E, respectively. Because of these six constraints, there are 11 free variables that described the system, and are chosen to be K, K_p, F, F_p, B, B_p, A, A_p, $[K_pF]$, $[F_pR]$, $[A_pE]$. The remaining variables can be expressed as a combination of

these variables and the total concentrations,

$$\begin{aligned}
[B_pA] &= A_T - A - A_p - [A_pE], \\
[F_pB] &= B_T - B - B_p - [B_pA], \\
[KTF_p] &= F_T - F - F_p - [F_pB] - [K_pF] - [F_pR], \\
[KT] &= K_T - K - K_p - [KTF_p] - [K_pF], \\
R &= R_T - [F_pR], \\
E &= E_T - [A_pE].
\end{aligned}$$

The equations corresponding to these reactions are

$$\begin{aligned}
\frac{dK}{dt} &= -Tk_1K + k_{1p}[KT] + \nu_K[K_pF], \\
\frac{dK_p}{dt} &= k_s[KT] - k_2K_pF + k_{2p}[K_pF], \\
\frac{dF}{dt} &= -k_2K_pF + k_{2p}[K_pF] + \nu_P[KTF_p] + k_5p[F_pB] - k_5FB_p + \nu_R[F_pR], \\
\frac{dF_p}{dt} &= \nu_K[K_pF] - k_3[KT]F_p + k_{3p}[KTF_p] - k_4F_pB + k_{4p}[F_pB] - k_8F_pR + k_8p[F_pR], \\
\frac{dB}{dt} &= -k_4F_pB + k_{4p}[F_pB] + k_{7p}[B_pA] - k_7BA_p, \\
\frac{dB_p}{dt} &= k_{5p}[F_pB] - k_5FB_p - k_6B_pA + k_{6p}[B_pA], \\
\frac{dA}{dt} &= -k_6B_pA + k_{6p}[B_pA] + \nu_E[A_pE], \\
\frac{dA_p}{dt} &= k_{7p}[B_pA] - k_7BA_p - k_9A_pE + k_{9p}[A_pE], \\
\frac{d[K_pF]}{dt} &= k_2K_pF - (k_{2p} + \nu_K)[K_pF], \\
\frac{d[F_pR]}{dt} &= k_8F_pR - (k_{8p} + \nu_R)[F_pR], \\
\frac{d[A_pE]}{dt} &= k_9A_pE - (k_{9p} + \nu_E)[A_pE].
\end{aligned}$$

Here, the rate constants assigned to the different reactions are as follows,

i. Autophosphorylation of K: k_1,k_{1p} are the association-dissociation rates for the reaction intermediate $[KT]$, and k_s is the rate of formation of K_p from this reaction intermediate.

ii. Phosphotransfer from K_p to F: k_2,k_{2p} are the association-dissociation rates for the reaction intermediate $[K_pF]$, and ν_K is the rate of formation of F_p from this reaction

intermediate.

iii. Dephosphorylation of F_p by $[KT]$: k_3,k_{3p} are the association-dissociation rates for the reaction intermediate $[KTF_p]$, and ν_P is the rate of formation of F from this reaction intermediate.

iv. Phosphotransfer from F_p to B: k_4,k_{4p} are the association-dissociation rates for the reaction intermediate $[F_pB]$ from the reactants F_p and B.

v. Reverse phosphotransfer from B_p to F: k_5,k_{5p} are the association-dissociation rates for the reaction intermediate $[F_pB]$ from the reactants B_p and F.

vi. Phosphotransfer from B_p to A: k_6,k_{6p} are the association-dissociation rates for the reaction intermediate $[B_pA]$ from the reactants B_p and A.

vii. Reverse phosphotransfer from A_p to B : k_7,k_{7p} are the association-dissociation rates for the reaction intermediate $[B_pA]$ from the reactants A_p and B.

viii. Dephosphorylation of F_p by R: k_8,k_{8p} are the association-dissociation rates for the reaction intermediate $[F_pR]$, and ν_R is the rate of formation of F from this reaction intermediate.

ix. Dephosphorylation of A_p by E: k_9,k_{9p} are the association-dissociation rates for the reaction intermediate $[A_pE]$, and ν_E is the rate of formation of A from this reaction intermediate.

Parameter values are based on [54], $k_1 = k_2 = k_3 = 1/(nM \cdot hr) = k_4 = k_5 = k_6 = k_7 = k_8 = k_9$,$k_{1p} = k_{2p} = k_{3p} = \nu_K = \nu_P = 10^3/hr = k_{4p} = k_{5p} = k_{6p} = k_{7p} = k_{8p} = k_{9p} = \nu_R = \nu_E$,$k_s = 10^2/hr$,$A_T = B_T = F_T = K_T = 1000nM$,$E_T = R_T = 100nM$ The steady state for different total concentrations of Spo0F is computed by numerically integrating these equations using ode23s (Supp. Fig. C.2e). For the computation with no reverse phosphotransfer, the corresponding rate constants are set to zero, $k_5 = k_7 = k_{4p} = k_{6p} = 0$. Similarly, for the computation with no Spo0F phosphatase, the corresponding parameters are set to zero, $R_T = k_8 = k_{8p} = \nu_R = k_3 = k_3p = \nu_P = 0$. In addition, there is an additional constraint as the reaction intermediate $[KTF_p]$ does not exist. Enforcing this constraint ($[KTF_p] = 0$) reduces the number of differential equations by one as the value of another reaction intermediate $[K_pF]$ is already determined, $[K_pF] = F_T - F - F_p - [F_pB] - [F_pR]$.

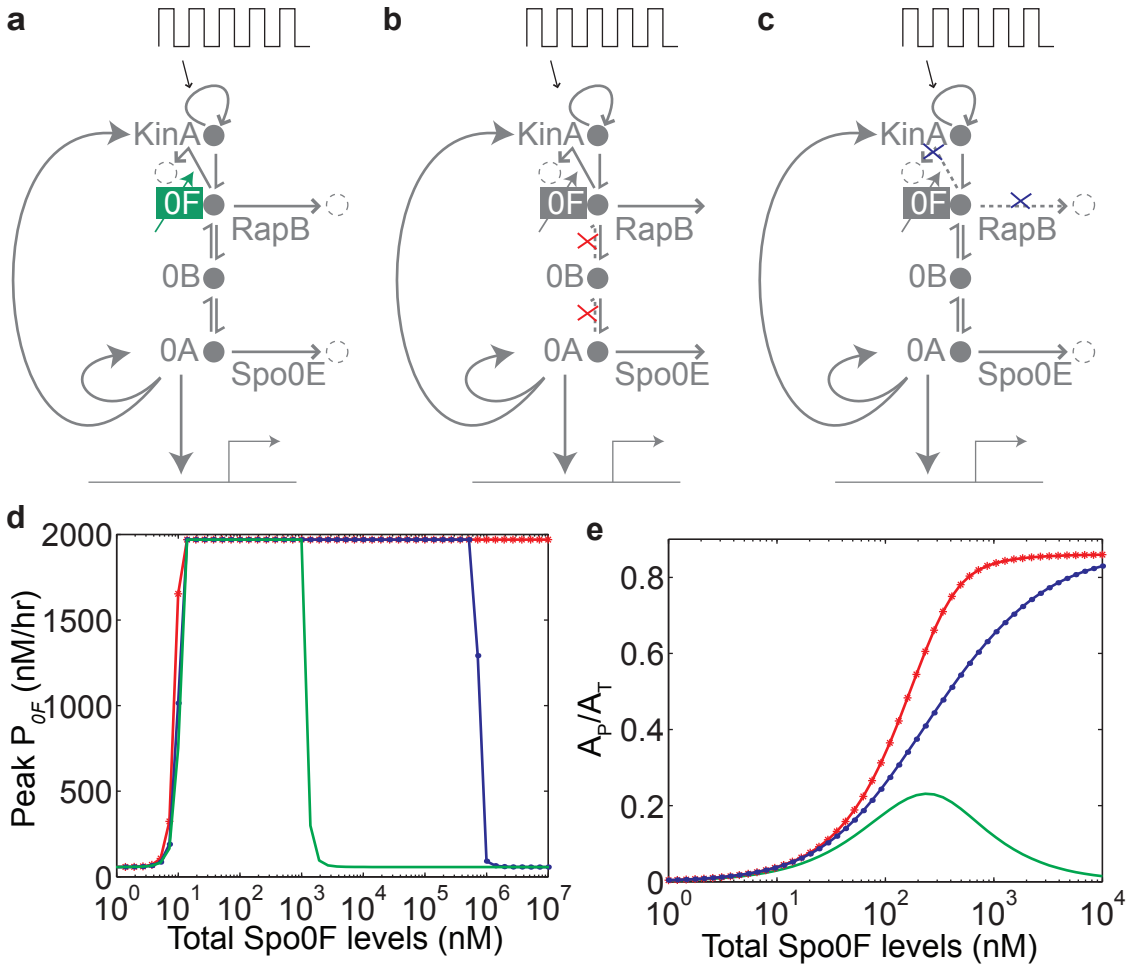

Figure C.2: Post-translational Spo0F bandpass in the full model with transcriptional feedback and pulsing or in the more complicated model of the core phosphorelay is due to the drain of Spo0A phosphates via reverse phosphotransfer and Spo0F phosphatase. Diagrams of the phosphorelay circuit (a) and versions with no reverse phosphotransfer (b, red) and no Spo0F phosphatase (c, blue), for which the post-translational Spo0F bandpass computation is performed from the full model described in the main text (including pulsing and transcriptional feedbacks, Fig. 2.7). Peak P_{0F} pulse amplitudes are plotted for different Spo0F induction levels (at steady state) for three cases: base parameters (d, green), no reverse phosphotransfer (d, red), and no Spo0F phosphatase (d, blue). The absence of Spo0F phosphatases shifts the repression threshold to significantly higher Spo0F values, representing drain of Spo0F phosphates by dilution due to cell growth. (e) Green curve is the post-translational Spo0F bandpass computed from a more complicated version of the core phosphorelay, described in the supplementary text. The computation is repeated in the absence of reverse phosphotransfer (red) and Spo0F phosphatases (blue).

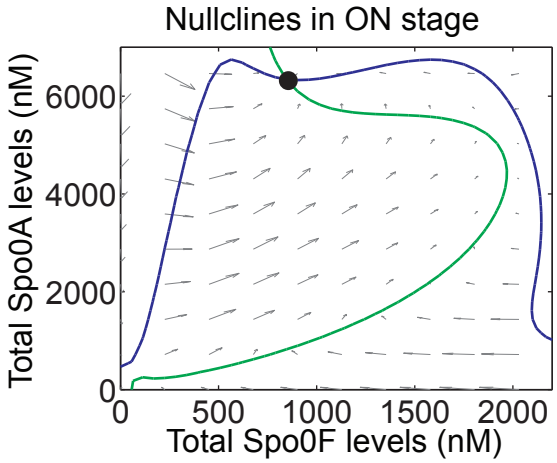

Figure C.3: Qualitative dynamic picture under the $P_{kinA} = P_{0A}$ assumption is similar to the alternate $P_{kinA} = P_{0F}$ assumption. Nullclines in the "ON" stage in the case when $P_{kinA}(A_p) = P_{0F}(A_p)$ are similar to the case discussed in 2.3 with the assumption that $P_{kinA}(A_p) = P_{0A}(A_p)$, suggesting that this assumption is justified. These nullclines are plotted for same parameters as used in the main text with $k_s(ON) = 110/hr$.

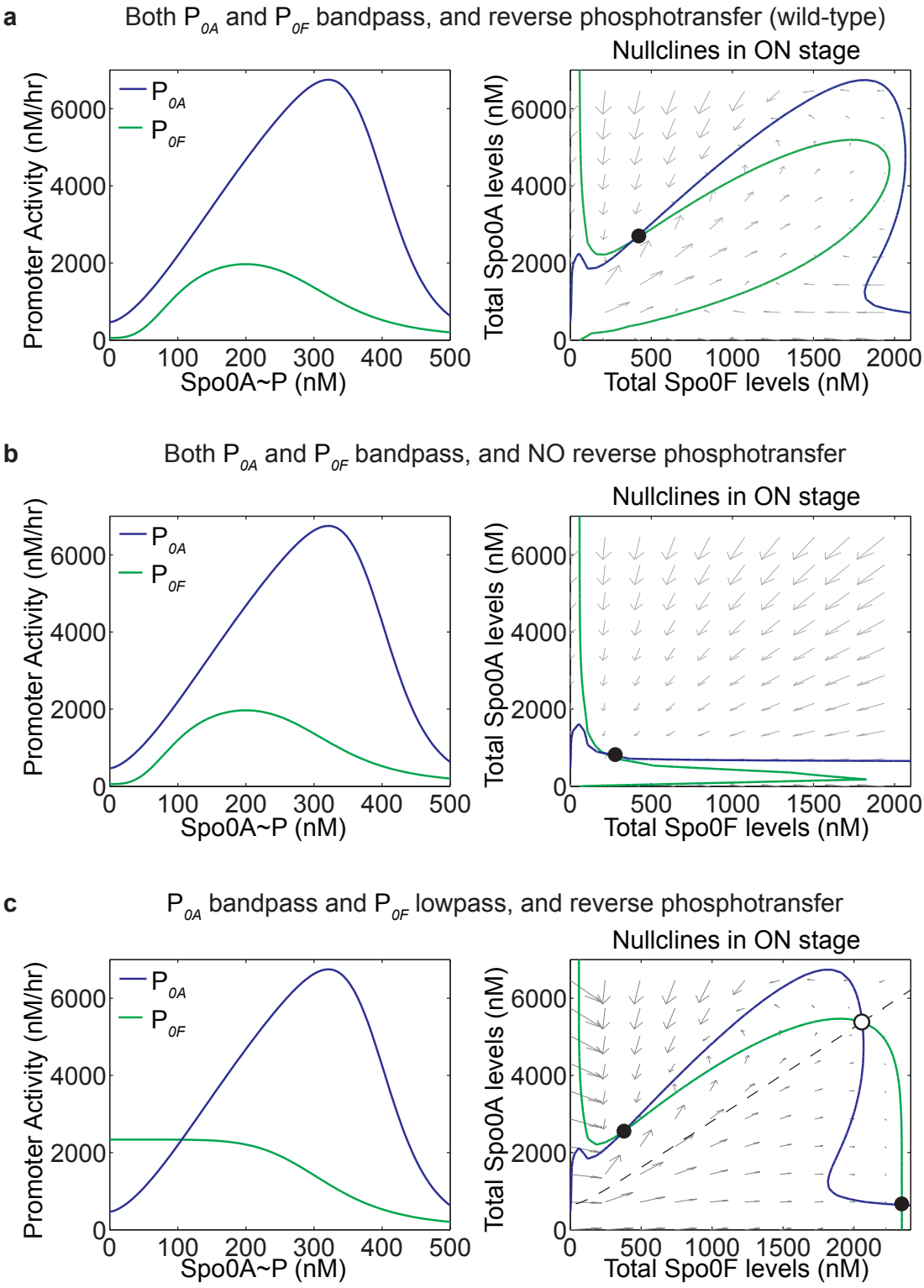
a
Both P0A and P0F bandpass, and reverse phosphotransfer (wild-type)
Nullclines in ON stage
Promoter Activity (nM/hr)
P0A
P0F
Spo0A~P (nM)
Total Spo0A levels (nM)
Total Spo0F levels (nM)
b
Both P0A and P0F bandpass, and NO reverse phosphotransfer
Nullclines in ON stage
c
P0A bandpass and P0F lowpass, and reverse phosphotransfer
Nullclines in ON stage

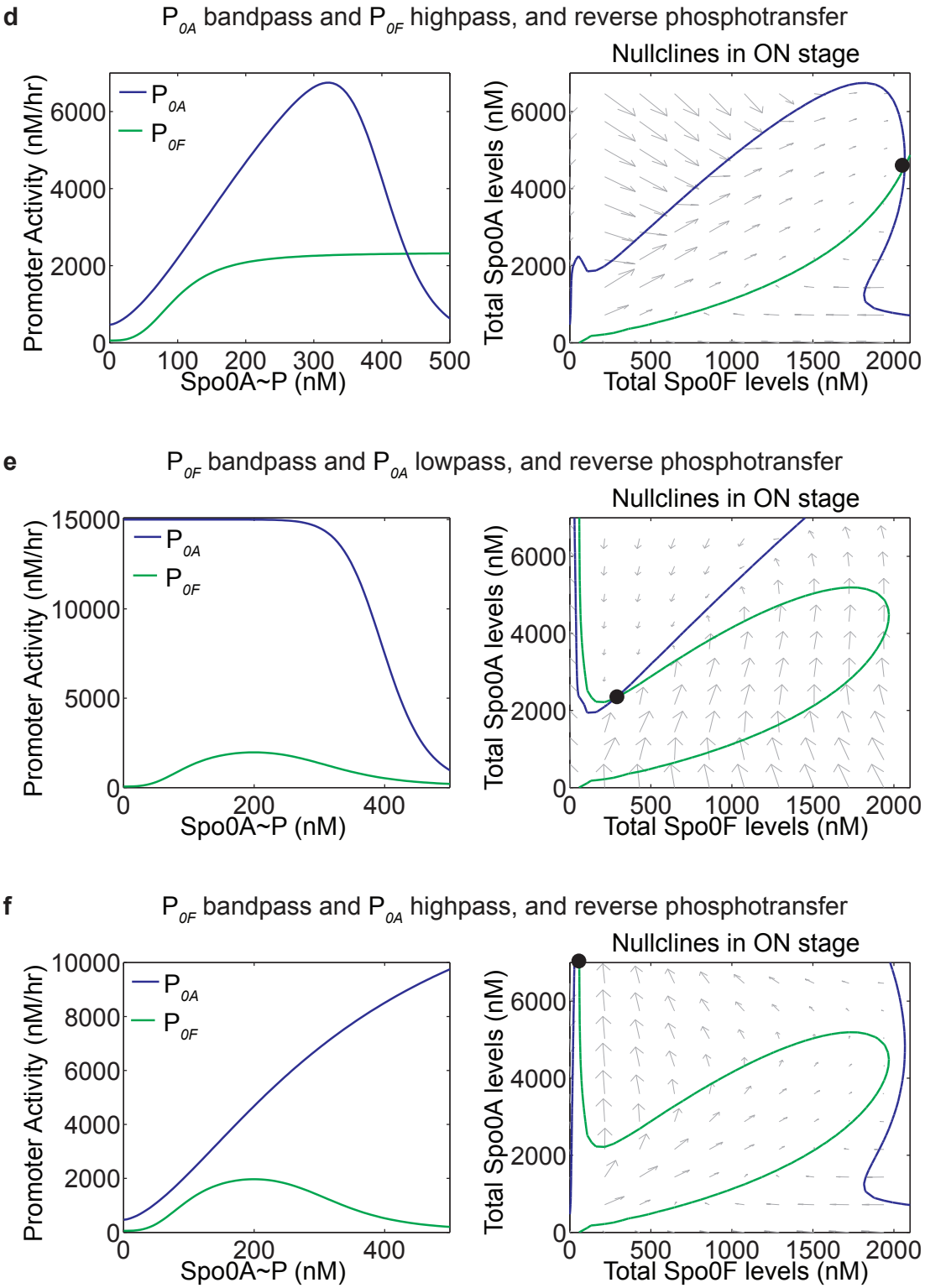
d
P0A bandpass and P0F highpass, and reverse phosphotransfer
Nullclines in ON stage
P0A
P0F
Promoter Activity (nM/hr)
Spo0A~P (nM)
Total Spo0A levels (nM)
Total Spo0F levels (nM)
e
P0F bandpass and P0A lowpass, and reverse phosphotransfer
Nullclines in ON stage
P0A
P0F
Promoter Activity (nM/hr)
Spo0A~P (nM)
Total Spo0A levels (nM)
Total Spo0F levels (nM)
f
P0F bandpass and P0A highpass, and reverse phosphotransfer
Nullclines in ON stage
P0A
P0F
Promoter Activity (nM/hr)
Spo0A~P (nM)
Total Spo0A levels (nM)
Total Spo0F levels (nM)

Figure C.4: Effect of bandpass characteristics on the alternate state. The effect of bandpass characteristics on the alternate state are investigated by comparing "ON" phase planes in the following cases, (a) Both P_{0A} and P_{0F} bandpass, and reverse phosphotransfer (wild-type case from Fig. 2.8, considered in 2.3) (b) Both P_{0A} and P_{0F} bandpass, and NO reverse phosphotransfer: Transcriptional bandpasses remain the same as case (a), but there is no post-translational bandpass. Nullclines orient differently from case (a), so that the alternate state doesn't exist and its effect on dynamics is minimal. (c) P_{0A} bandpass, P_{0F} lowpass (only repression), and reverse phosphotransfer: Nullclines are slightly perturbed from case (a), with the appearance of a stable steady state, an unstable steady state (white circle), and the associated separatrix. The separatrix is computed by integrating equations backward in time starting from an initial condition near the unstable steady state. The additional stable steady state is similar in location to the alternate state. (d) P_{0A} bandpass, P_{0F} highpass (only activation), and reverse phosphotransfer: Nullclines are slightly perturbed from case (a), with the stable steady state situated like the alternate state. (e) P_{0F} bandpass, P_{0A} lowpass (only repression), and reverse phosphotransfer: Nullclines are slightly perturbed from case (a), but without significant change in the steady state location. (f) P_{0F} bandpass, P_{0A} highpass (only activation) and reverse phosphotransfer: Nullclines are slightly perturbed from case (a), but without significant change in the steady state location. In this case, the stable steady state is situated above the upper Y-axes limit.